

# Accurate Single-Molecule Kinetic Isotope Effects

Yilin Guo,<sup>▽</sup> Chen Yang,<sup>▽</sup> Huiping Li,<sup>▽</sup> Lei Zhang,<sup>▽</sup> Shuyao Zhou, Xin Zhu, Huanyan Fu, Zhizhou Li, Zhirong Liu, Chuancheng Jia, Zitong Liu,\* Wenguang Zhu,\* Fanyang Mo,\* Deqing Zhang,\* and Xuefeng Guo\*



Cite This: *J. Am. Chem. Soc.* 2022, 144, 3146–3153



Read Online

ACCESS |



Metrics & More



Article Recommendations



Supporting Information

**ABSTRACT:** An accurate single-molecule kinetic isotope effect (sm-KIE) was applied to circumvent the inherent limitation of conventional ensemble KIE by using graphene–molecule–graphene single-molecule junctions. *In situ* monitoring of the single-molecule reaction trajectories in real time with high temporal resolution has the capability to characterize the deeper information brought by KIE. The C–O bond cleavage and the C–C bond formation of the transition state (TS) were observed in the Claisen rearrangement through the secondary kinetic isotope effect, demonstrating the high detection sensitivity and accuracy of this method. More interestingly, this sm-KIE can be used to determine TS structures under different electric fields, revealing the multidimensional regulation of the TS. The detection and manipulation of the TS provide a broad perspective to understand and optimize chemical reactions and biomimetic progress.



## INTRODUCTION

Insights into reaction mechanisms contribute to optimizing synthetic routes and realizing significant cost savings in laboratory preparation and industrial production. In particular, an understanding of the rate-determining step (RDS) is of crucial importance to high reaction yield and efficiency. As an effective method to demonstrate the transition state (TS) configuration and the RDS, KIE has been applied in many reactions for mechanism studies,<sup>1–3</sup> exemplified by studies into the aromatic nucleophilic substitution reaction (<sup>12</sup>C/<sup>13</sup>C KIE),<sup>4</sup> the Morita–Baylis–Hillman reaction (primary H/D KIE, involving the cleavage/formation of O–H/C–H bonds),<sup>5</sup> and the Claisen rearrangement (secondary H/D KIE, involving the cleavage/formation of O–C/C–C bonds).<sup>6–15</sup> In general, when the overall reaction rate changes as a consequence of switching isotopes, the isotope substitution site is likely to participate in the RDS to a greater extent (primary isotope effect) or to a lesser extent (secondary isotope effect), thereby helping to determine the main reaction trajectories and corresponding TS structures. However, it is hard to precisely measure KIEs because the KIE values are generally close to 1 (not much difference between the values).<sup>1</sup>

As the reaction progresses, the reactants with a slower reaction rate are continuously accumulated. Therefore, when the reaction is nearing completion, the relative concentration of the reactant containing heavy-atom isotopes will increase. The relationship among the ratio of the isotope content in the reclaimed reactant to the isotope content in the reactant at the beginning ( $R/R_0$ ), the extent of a reaction ( $F$ ), and the KIE obeys eq 1:<sup>1</sup>

$$\frac{R}{R_0} = (1 - F)^{1/\text{KIE}-1} \quad (1)$$

In these experiments, nuclear magnetic resonance spectroscopy (NMR) is used to measure the content of <sup>2</sup>H and <sup>13</sup>C in the reactant. The KIE of each center can be measured by substituting the isotopic content ratio of each carbon atom or hydrogen atom into the above formula. However, this method is significantly limited by the naturally low abundance of isotopes and the extent of the reaction, resulting in low sensitivity and poor accuracy. In addition, the interpretation of experimental measurements of KIEs requires a known mechanism; otherwise, it may lead to inappropriate conclusions.<sup>16</sup> Therefore, taking advantage of KIEs to realize the visualization of intrinsic reaction pathways is an urgent and key challenge that needs to be solved.

Single-molecule detection (SMD) can shed light on the inherent laws of a reaction,<sup>17</sup> which is expected to be an ideal strategy to break through this bottleneck. SMD presents us with the opportunity to directly visualize the reaction process and possibly noteworthy KIEs, without being limited by abundance. To date, various kinds of SMDs based on molecular optical,<sup>18,19</sup> mechanical,<sup>20,21</sup> and electrical<sup>22,23</sup> properties have flourished for decades. Numerous single-

Received: November 27, 2021

Published: January 17, 2022



molecule effects, such as the field-induced effect,<sup>24</sup> the Kondo effect,<sup>25</sup> the Coulomb block,<sup>26</sup> negative differential conductance,<sup>27</sup> and quantum interference,<sup>28</sup> have been discovered and studied. However, few studies of KIEs on single molecules have been reported,<sup>29</sup> due to the limited inherent accuracy of monitoring chemical reactions. In contrast, the platform of graphene–molecule–graphene single-molecule junctions (GMG-SMJs)<sup>22,30–32</sup> provides unprecedented accurate measurements of chemical reactions<sup>33–35</sup> and intermolecular interactions,<sup>36–38</sup> which lays the foundation to study the KIE effect on single-molecule reactions. In this work, we applied sm-KIE to probe the detailed properties of each intermediate in the Claisen rearrangement reaction and thus discover unexpected reaction behaviors (beyond the traditional textbook understanding) from their intrinsic dynamics.

## RESULTS AND DISCUSSION

**Device Fabrication and Characterization.** From the perspective of molecular engineering, phenol-based GMG-SMJs were prepared by covalently integrating a designed molecular bridge with a phenol functional center and amino terminals into nanogapped carboxyl-terminated graphene point electrodes (Figure 1A and Schemes S1 and S2). To confirm the successful formation of the single-molecule device, we compared the current–voltage ( $I$ – $V$ ) curves before and after the connection of the molecular bridge, as shown in Figure S1. About 16 of 169 devices showed the successful connection ( $\sim 10\%$  yield) and  $\sim 95\%$  probability of only one-molecule integration between two electrodes could be demonstrated by statistical analysis in the Supporting Information. Furthermore, under a constant bias voltage (300 mV), the bistable switching model between the low and high current levels in recorded  $I$ – $t$  curves in an alkaline environment (Figure 1B) originates from the conversion of phenol and phenoxy anion. Those were demonstrated by their corresponding low and high electron transmission probabilities (Figure 1B and Figure S2). This also elucidated the successful connection of the phenol functional molecular bridge. In addition, the bistable switching in alkaline concentration-dependent measurements (Figure S3) showed the preference for the phenoxy anion in an alkali-rich environment, which can be used as a nucleophile to react with allyl bromide to synthesize the substrate for a Claisen rearrangement at the single-molecule level. In advance, a fluorescein-substituted allyl bromide was added in order to visualize the synthesis at the single-molecule site. The fluorescent blinking at the single-molecule site results from the repeated combination (fluorescence quenched by graphene electrodes)—dissociation (fluorescence on) between the fluorescent substrates and the phenoxy anion. This process was captured by a stochastic optical reconstruction microscopy (STORM) technology.<sup>39</sup> The 100% probability of the appearance of only one fluorescence point between electrodes in single-molecule devices (Figure 1C) via a super-resolution microscope and STORM proved the successful incorporation of allyl fluorescein species and provided direct experimental evidence of only one molecular connection in our devices. More importantly, the highly correlated fluorescent intensity and current signals (Figure 1D and the supplementary movie) provided further strong evidence that the observed signals indeed resulted from the single-molecule phenol and its derivative.<sup>40</sup> The detailed mechanism is shown in Figure S4.

**Claisen Rearrangement.** To monitor a single-molecule Claisen rearrangement, we added allyl bromide to the device

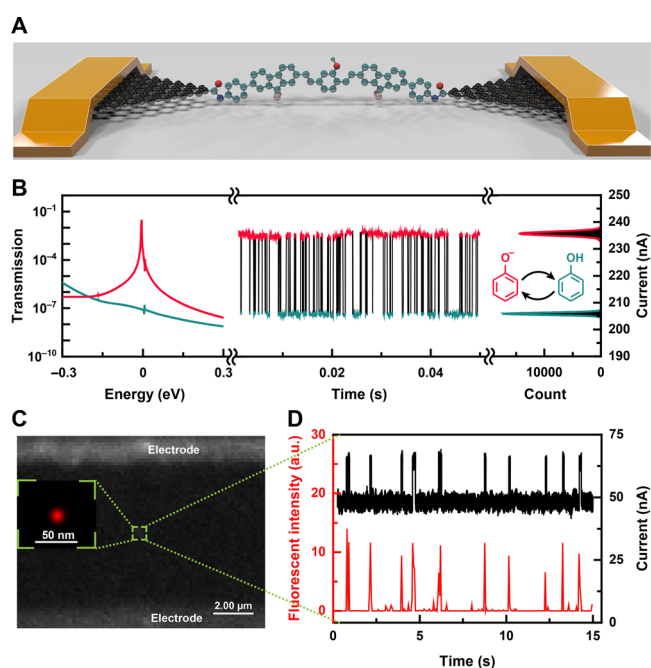


**Figure 1.** Device structure and characterization of phenol-based GMG-SMJs. (A) Schematic diagram of a phenol-based single-molecule device. (B)  $I$ – $t$  curves of the device in an alkaline environment ( $1 \times 10^{-2}$  mol/L NaOH solution), the corresponding histogram (right, showing bistable states), and the corresponding transmission spectra of phenol and phenoxy anion (Figure S2). In comparison with the phenol form, for the phenoxy anion form, the perturbed highest occupied molecular orbital ( $p$ -HOMO) has a transmission peak with an energy much closer to that of the unbiased electrode chemical potentials ( $E_F$ ), leading to the higher conductance. (C) Characterization of a single-molecule connection. During the interaction between a single-molecule phenoxy anion and a fluorescein-substituted allyl compound, 5000 photos taken by a super-resolution fluorescence microscope with 50 ms exposure are reconstructed to obtain a single-molecule resolution photograph and enlarged image without the background. (D) Synchronous monitoring of current and fluorescent (the mean intensity of fluorescence in the region of the single-molecule functional center) signals.

under alkaline conditions to produce allyl phenyl ether and monitored the current level at 300 mV bias voltage. An irreversible change in the current shows the  $S_N2$  substitution of allyl bromide and successful preparation of allyl phenyl ether (Figure S5). Next, we replaced the solvent with a solution of  $10^{-3}$  mol/L trifluoroacetic acid (TFA) and further monitored the acid-catalyzed Claisen rearrangement. At the beginning, two conductance states were observed at room temperature, implying the reversible protonation of the allyl phenyl ether reaction substrate (RS) due to the relatively high energy barrier of the Claisen rearrangement (usually heating to 60–200 °C at macroscopic scales). The TFA concentration dependence of the binary conductance switching (Figure S6) provided a support for this assignment. There was a greater amount of the low-conductance state at higher TFA concentrations, illustrating that it should correspond to the protonation state ( $RSH^+$ ) and the high-conductance state should be assigned to the RS itself. Then, the reaction temperature was raised to 100 °C, and the  $I$ – $t$  curves were recorded with six distinct conductance states (Figure 2A). Control experiments performed by replacing the allyl bromide solution with a 1-bromopropane solution are provided in

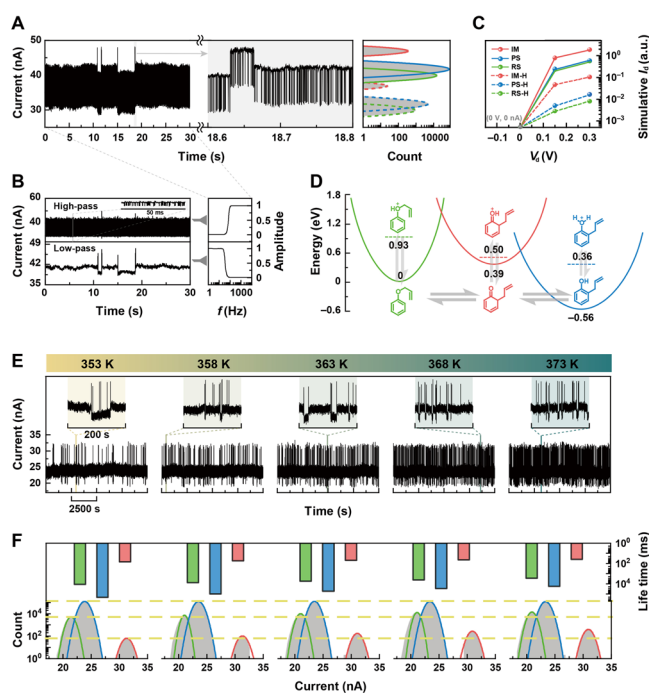


**Figure 2.** Characterization of a single-molecule Claisen rearrangement. (A) Recorded  $I-t$  curves of the Claisen rearrangement, an enlarged image, and the corresponding histogram (30 s). (B) Electrical signals via high-pass and low-pass filtering of the  $I-t$  curves in (A), respectively. The filter settings are provided on the right. (C) Simulated  $I_d$  values of six possible species during the Claisen rearrangement, corresponding to the six conductance states in (A). (D) Energy profiles of the six species and their conversion relationships. (E) Recorded  $I-t$  curves (low sampling rates) at different temperatures and the corresponding enlarged images. (F) Corresponding lifetimes of each state and the histograms at different temperatures.

**Figure S7.** Only two conductance states were monitored, implying the reversible conversion between the propane phenyl ether and the protonated propane phenyl ether and verifying that no Claisen rearrangement occurs.

To better analyze the current data, we used the Butterworth filtering method to perform high-pass and low-pass filtering to distinguish signals. The electrical signals that meet the specific frequency (low or high bands) were amplified (amplitude–frequency response, Figure 2B right), and by doing so, two electrical signal modes were obtained. One was the high-pass-filtered binary switching signal, and the other was the low-pass-filtered signal corresponding to relatively slow conversions and showing three main conductance states (Figure 2B). Through an analogy to the raw signal, the high-pass-filtered signal can be assigned to the conversion between the three lower states (the dashed line in the corresponding histogram) and others (Figure 2A). The one-mode conversion in the high-pass-filtered signal shows that these three states were derived from the same reaction events, which can be assigned to the protonation and corresponding dissociation. The conversion rates ( $\sim \mu\text{s}^{-1}$ ) of the protonation process (Figure S6) also met at the cutoff frequency (1 kHz), which supports this assignment. Then, the other low-pass-filtered signal can be assigned to the Claisen rearrangement at 100 °C. The relatively low reaction rates in the macroscopic experiment<sup>41</sup> also were in accordance with a frequency less than 1 kHz. The species with the highest conductance can be transformed into

two lower-conductance species, while these two conductance states cannot be transformed into each other (Figure 2B, left), implying that the highest conductance state was an inevitable intermediate during the reaction. The electron transmission spectra and potential energies of the RS, product state (PS), and possible intermediate state (IM) were also studied (Figure 2C, Figure S8, and Figure 2D). The simulated conductances from low to high were RS, PS, and IM (Figure 2C). In addition, the corresponding protonated species were found to have the same order but an overall lower order in comparison to the neutral species (Figure 2C), which is consistent with the previous TFA-dependent measurements (Figure S6) and the high-pass signals (Figure 2B). Similarly, the theoretical studies of the energy profiles showed that the sequence of the potential energy of the neutral species from low to high was PS, RS, and IM (Figure 2D), which matches their dwell times in the low-pass signals (Figure 2B). All of the corresponding protonated species have relatively high energies, demonstrating less probability of occurrence as shown in Figure 2A. On the basis of the filtering method, the different chemical reaction processes were distinguished conveniently.

In view of the slow rate of the Claisen rearrangement process,<sup>41</sup> the number of events exhibited by 57600 Hz is few unless the acquisition time is greatly extended, which will create a large amount of data and make data processing difficult. Fortunately, the splitting of electrical signals can also be approached at the instrument and the Claisen rearrangement can be monitored via a reduced bandwidth (57.6 Hz). Therefore, the Claisen rearrangement can be observed more intuitively and the problem of excessive data volume caused by the high sampling rate can be avoided. The temperature-dependent measurements further prove the availability of the single-molecule platform and the accuracy of determining kinetic and thermodynamic properties, laying the foundation for sm-KIE measurements. The Claisen rearrangement at five different temperatures (353, 358, 363, 368, and 373 K) were recorded (Figure 2E). The ratios of the peak areas in the histograms and the lifetimes (derived from statistics of each time interval) of each state reflect the change in thermodynamics and kinetics with temperature (Figure 2F). The positive correlation between the ratio RS/PS and temperature reveals an overall exothermic reaction ( $\Delta H < 0$ ). More quantitative analysis is provided in Figure S9. In addition, the shorter lifetime of each state at higher temperatures demonstrates the acceleration of each elementary step. Furthermore, the reaction rate constants  $k = 1/\tau$  ( $\tau$  is the lifetime) were found to have a linear relationship with  $1000/T$ , meeting the Arrhenius equation. Thus, the activation energy  $E_a$  can be derived (Figure S10). A quantitative analysis shows that the single-molecule electrical detection platform has sufficient capacity to study the KIE.

**Single-Molecule KIE.** On the basis of the visualized trajectories and the detected intermediate (IM) discussed above, the 3,3- $\sigma$ -migration process (RS to IM), which is slower than the proton shuttle (IM to PS), can be directly determined as an RDS (rather than via ensemble KIE). Further studies of the KIE of the elementary step (3,3- $\sigma$ -migration) contribute to a deeper understanding of the mechanism. We synthesized two allyl compounds with different deuterated positions, which reacted with the phenoxy anion through nucleophilic substitution, respectively, to generate Claisen rearrangement substrates: allyl phenyl ethers  $\text{sp}^2\text{-D}$  (deuterium connected to  $\text{sp}^2$  C) and  $\text{sp}^3\text{-D}$  (deuterium connected to  $\text{sp}^3$  C) (Figure

3A–C). Under experimental conditions identical with those above, electrical measurements were performed on these

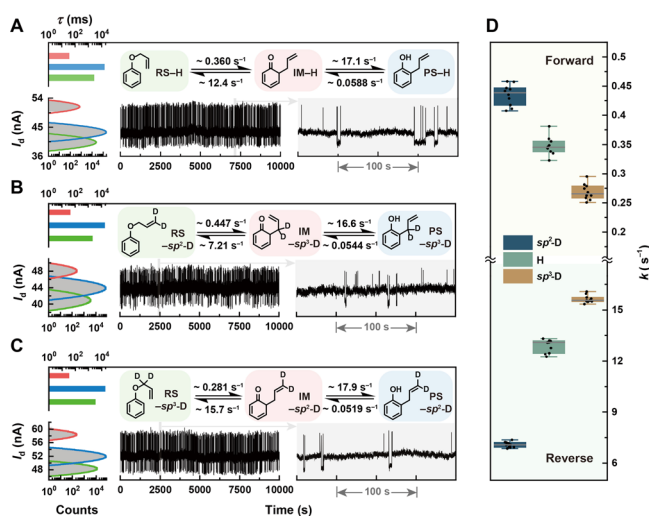


**Figure 3.** Characterization of sm-KIE. (A–C)  $I$ – $t$  curves and corresponding enlarged images of single-molecule nondeuterated (A),  $sp^2$ -D (B) and  $sp^3$ -D (C) substrates. The corresponding lifetimes of each state and histograms are provided in the pictures on the left, respectively. The estimated reaction rate constants of each elementary step are provided on the top, respectively. (D) Box plots of the forward and reverse rate constants of 3 kinds of devices based on the statistics of 10 devices.

GMG-SMJs with three functional centers of nondeuterated (H),  $sp^2$ -D and  $sp^3$ -D. In comparison with the nondeuterated reaction rates, the changes in the reaction rate of  $sp^2$ -D and  $sp^3$ -D are not noticeable in the inset histograms of the lifetime,  $\tau$ . Similarly, the statistics of the ratios of each conductance state vary very little among the three kinds of devices, revealing a slight effect on the kinetics and thermodynamics by isotopic substitution, which is consistent with the ensemble experiments. However, the subtle difference can be shown with the quantitative analysis by a maximum interval likelihood rate estimate. At 373 K, we tested 10 additional devices for each reaction center to obtain the conversion rate constant ( $k$ ) of each elementary step at 300 mV, including the rate constant of the 3,3- $\sigma$ -migration process in the Claisen rearrangement (RS to IM, abbreviated as  $k_C$ ), as shown in Figure 3A–C and Figures S11–S39. The box plots of the rate constants ( $k_C$ s) of 3,3- $\sigma$ -migration in the rearrangement process (RS to IM) are provided in Figure 3D. All three kinds of devices revealed obvious differences in both the forward and reverse 3,3- $\sigma$ -migrations, while there is only a slight difference in the proton shuttle (Figure S40). This also proves the correctness of the conductance state assignment. In addition, obvious solvent KIEs were found in the proton shuttle progress (Figure S41), providing more opportunities for our platform to further detect solvent effects and proton transformation at the single-molecule level (which are not the focus of the current study). According to the definition of the kinetic isotope effect, the KIE values of the forward and reverse reactions of  $sp^2$ -D and  $sp^3$ -D are obtained, as shown in Table S1. For the forward reaction, the KIE value of  $sp^2$ -D is less than 1, while the KIE value of  $sp^3$ -D is greater than 1, which is consistent with the KIE theory. The resistance to the bending vibration decreases as the carbon atom undergoes a change from  $sp^3$  to  $sp^2$

hybridization, which has a greater influence on the C–H bond than on the C–D bond, leading to the difference in the activation energy of the reaction. Therefore, the reaction rate decreases when the C–H bond is replaced by the C–D bond ( $k_H/k_{sp^3-D} > 1$ ). Conversely, when a carbon atom undergoes a change from  $sp^3$  to  $sp^2$  hybridization, the reaction rate increases ( $k_H/k_{sp^2-D} < 1$ ). Specifically, the sm-KIE values at a general bias voltage (300 mV) and 373 K are  $k_H/k_{sp^2-D} = 0.798 \pm 0.004$  and  $k_H/k_{sp^3-D} = 1.290 \pm 0.060$ , which are more obvious than the results ( $k_H/k_{sp^2-D} = 0.950 \pm 0.020$  and  $k_H/k_{sp^3-D} = 1.180 \pm 0.020$ ) in previous work on the aromatic Claisen rearrangement at 443–468 K.<sup>13</sup> The more obvious KIE at the single-molecule level can be attributed to three main reasons. (1) Due to the catalysis by an acid, we conducted the single-molecule Claisen rearrangement at a relatively low temperature (373 K). According to  $\frac{k_H}{k_D} = \frac{A_H}{A_D} e^{-[\Delta E_a]_D^H/RT}$  showing an inverse proportion to some extent,<sup>42</sup> the lower temperature leads to a larger KIE. (2) Without the influence of the natural abundance and the difference in the reaction extent between H- and D-substituted substrates, the pure single (isotope substituted) molecule shows a more obvious KIE. (3) The focused single-molecule phenol moiety was necessarily substituted at the 2- and 5-positions to span the gap. The KIE of the Claisen rearrangement was reported to have a large substitution effect,<sup>9</sup> which results in the difference between ensemble and single-molecule measurements.

**Regulation of the Transition State.** According to KIE =  $EIE^i$  ( $EIE$  is the equilibrium isotope effect,  $EIE = \frac{K_H}{K_D}$  and  $i$  is the breakage or formation degree on the corresponding deuterated carbon),<sup>43</sup>  $i$  can be derived from the simple formulas

$$EIE = \frac{k_{+H}k_{-D}}{k_{+D}k_{-H}} = \frac{KIE_+}{KIE_-} \quad (2)$$

$$i = \frac{\ln KIE_+}{\ln KIE_+ - \ln KIE_-} \quad (3)$$

For  $sp^2$ -D,  $i \approx 27\%$ , which means that the C–C bond formation degree is  $\sim 27\%$ . For  $sp^3$ -D, the degree of C–O bond cleavage is  $\sim 57\%$  (the calculation process of  $i$  is provided in the Supporting Information). These reveal the structure of the TSs: the cleavage degree of the C–O bond is greater than the formation of the C–C bond, which proves the concerted but asynchronous mechanism of 3,3- $\sigma$ -migration. Note that the derived  $i$  represents not only the C–C and C–O bond stretching but also the variations of the vibrational frequencies in the reaction coordinate. Specifically, the C–H vibrational frequencies (such as the transition of the out-of-plane bending vibration between  $sp^2$  and  $sp^3$  carbons) resulting from the change in the type of carbon hybridization during the reaction can be reflected in the observed KIE. The derived  $i$  implies the change degree of the labeled C–H bond vibration frequency from the substrate to the TS. A higher value was found on the  $sp^3$  carbon, showing more change in this C–H vibrational frequency and the type of the hybridization, which also implies a greater degree of the C–O bond breaking in comparison to the C–C bond formation. Moreover, the sum of bond breakage and bond formation is less than 1, indicating that the transition state is more like the substrate than the product and the reaction experiences an early transition state. To better describe the multidimensional view of the Claisen rearrange-

ment, a More O'Ferrall–Jencks diagram is provided in Figure S42, also revealing the concerted but asynchronous mechanism.

Due to the relatively high polarity of the TS in the 3,3- $\sigma$ -migration, water was found to accelerate the reaction.<sup>44</sup> In the current case, the natural external electric field (EEF)<sup>45,46</sup> in the single-molecule junction is considered to regulate the apparent reaction rates and TS structures. To identify the TS structure,  $I-t$  curves of three kinds of devices were recorded under different bias voltages (Figures S11–S39) and the corresponding rate constants and KIEs are provided in Tables S1 and S2. A set of  $I-t$  curves of the nondeuterated device is provided in Figure 4A. All of the forward reaction rate estimates show a

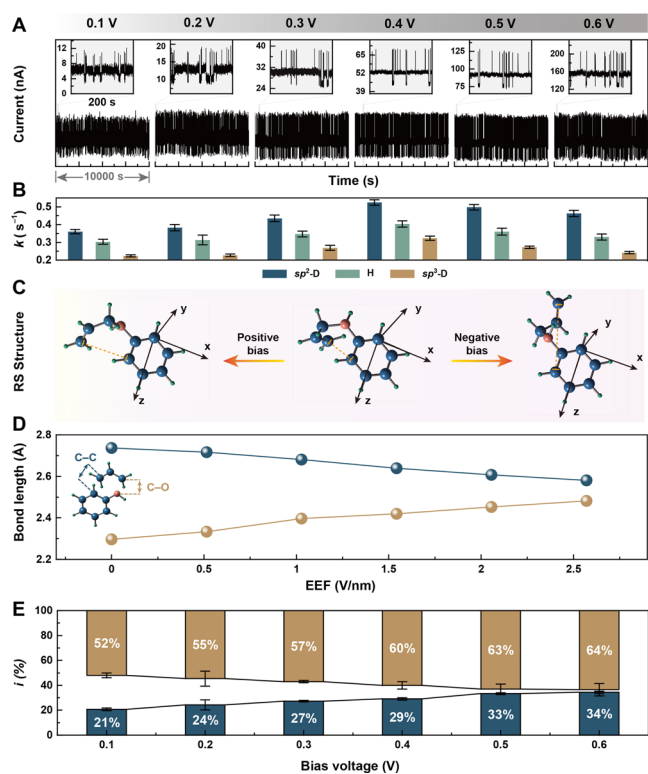


**Figure 4.** Bias-voltage-dependent measurements and regulation of TSs via EEFs. (A)  $I-t$  curves and corresponding enlarged images under different bias voltages. (B) Estimated  $k_{CS}$  of three kinds of devices under different biases, respectively. (C) Simulated TS structures under +5.14 V/nm (left, parallel to the Z axis), 0 V/nm, and -5.14 V/nm EEF (right, antiparallel to the Z axis) strengths. (D) Distances of the C–C and C–O bonds of simulated TSs under different EEFs. (E) Degrees of C–O bond breakage (brown) and C–C bond formation (dark blue) derived from sm-KIE under different biases.

nonmonotonic relationship between  $k_{CS}$  and the bias voltage (Figure 4B), implying a regulatory effect on the Claisen rearrangement. However, only one conductance (RS) was recorded when we switched the bias voltage direction, revealing no reaction of the substrate (Figure S43). The benzene ring was fixed and optimized under the electric field parallel to the molecular bridge (Z axis in Figure 4C). The spatial orientation of the allyl group connected by the C–O–C bond varies under different electric fields. The entire allyl group shifts away from the reaction site (the distance is marked as an orange dashed line) and is unable to form the six-membered ring TS required for rearrangement under a

negative bias (forming an electric field antiparallel to the Z axis), thus resulting in a no-reaction state. On the other hand, the structural change of the allyl group was restricted to the neighboring reaction site under the electric field parallel to the Z axis, which makes it easier to meet the requirement of rearrangement. In addition, the EEF plays a role in stabilizing the polar TS and further accelerates the reaction, as demonstrated by the positive correlation between  $k_{CS}$  and voltages at a low bias range (100–300 mV) in Figure 4B. However, when the EEF was further increased, the allyl groups were more strictly aligned in the direction of the electric field, and the structural change became difficult. Under these conditions, the orientation of the allyl group has changed to be in plane with a larger distance from the reaction site (Figure 4C, left), causing a certain deviation between its position and the TS as well as a relatively higher energy barrier. This is consistent with the negative correlation between  $k_{CS}$  and voltages at a high bias range (400–600 mV). The bias-voltage-dependent measurements reveal the regulation of the apparent reaction rates and both the forward and reverse catalysis by EEFs.

Furthermore, the bond length of the TS under different EEFs obtained from the theoretical studies provided evidence of the regulation of the TS structure via EEFs. With an increase in the applied electric field, the C–C bond's distance in the transition state gradually decreases, and the C–O bond's distance increases (Figure 4D). The computational results (the bond lengths and the atomic coordinates of TS) are provided in Tables S3–S8. The theoretical simulation has accuracy limitations, but the ultrasensitive single-molecule experiments provide a more accurate description. The breakage (C–O bond) or formation (C–C bond) degrees of the TS under different bias voltages were derived from the KIE of two kinds of deuterated devices (Figure 4E). As the bias voltage increases, the degree of the C–O bond breakage and the degree of the C–C bond formation gradually increase, indicating that the TS shifts to the right (the structure of the early TS is more similar to that of the product). At the same time, the sum of the degrees of both bond breakage and bond formation is less than 1, showing that the transition state is still more like a reactant than the product, and the reaction experiences an early transition state. The TS structure shows its position change along the reaction coordinate under different EEFs. In combination with the influence of the EEF on the height of the TS, we found the diversification of the EEF regulation: the molecular configuration, the energy barrier (orthogonal direction), and the TS position (horizontal direction). From another perspective, this sm-KIE approach offers a multidimensional description of the TS, the Holy Grail of chemical research, which forms the foundation of direct detection of the TS.

## CONCLUSION

In summary, we demonstrate sm-KIE as a distinctive method to reveal the intrinsic mechanism of chemical reactions. The filtering technology has been creatively used in distinguishing electrical signals, which allows us to analyze different reaction processes in one reaction data set and simultaneously determine the KIE of forward and reverse reactions. In addition to quantitative analyses of thermodynamics and kinetics of sm-KIE, different EEFs are also found to not only control the occurrence of the reaction but also realize the precise regulation of the TS structures. We firmly believe that,

with the advantages of high detection sensitivity and accuracy, this sm-KIE approach is ready to be applied immediately to a variety of single-molecule dynamics studies, which is crucial to the development of fundamental chemical reactions and an understanding of basic life sciences.

## ■ ASSOCIATED CONTENT

### SI Supporting Information

The Supporting Information is available free of charge at <https://pubs.acs.org/doi/10.1021/jacs.1c12490>.

Molecular synthesis, fabrication procedure of the graphene FET array and single-molecule device, single-molecule connection analysis,  $I$ – $V$  curves of single-molecule devices, transmission spectra of phenol and phenoxy anion, pretreatment of graphene–phenol–graphene junctions, photoelectrical integration, preparation of the substrate, protonation of the substrate, control experiment for single-molecule devices, the transmission spectra of six species, plots of thermodynamic and kinetic properties, additional  $I$ – $t$  curves of three kinds of devices, the summary of the rate constants and sm-KIEs, rate constants of the proton shuttle, the calculation process of  $i$ , a More O’Ferrall–Jencks diagram,  $I$ – $t$  curves under negative bias voltages, the bond lengths and the atomic coordinates of the TS, and the theoretical simulation methods (PDF)

Fluorescent intensity and current signals (MP4)

## ■ AUTHOR INFORMATION

### Corresponding Authors

**Zitong Liu** – State Key Laboratory of Applied Organic Chemistry, College of Chemistry and Chemical Engineering, Lanzhou University, Lanzhou, Gansu 730000, People’s Republic of China; Email: [liuzt@lzu.edu.cn](mailto:liuzt@lzu.edu.cn)

**Wenguang Zhu** – ICQD, Hefei National Laboratory for Physical Sciences at the Microscale, Department of Physics, University of Science and Technology of China, Anhui 230026, People’s Republic of China; [orcid.org/0000-0003-0819-595X](https://orcid.org/0000-0003-0819-595X); Email: [wgzhu@ustc.edu.cn](mailto:wgzhu@ustc.edu.cn)

**Fanyang Mo** – School of Materials Science and Engineering, Peking University, Beijing 100871, People’s Republic of China; Email: [fmo@pku.edu.cn](mailto:fmo@pku.edu.cn)

**Deqing Zhang** – Beijing National Laboratory for Molecular Sciences, CAS Key Laboratory of Organic Solids, Institute of Chemistry, Chinese Academy of Sciences, Beijing 100190, People’s Republic of China; [orcid.org/0000-0002-5709-6088](https://orcid.org/0000-0002-5709-6088); Email: [dqzhang@iccas.ac.cn](mailto:dqzhang@iccas.ac.cn)

**Xuefeng Guo** – Beijing National Laboratory for Molecular Sciences, National Biomedical Imaging Center, College of Chemistry and Molecular Engineering, Peking University, Beijing 100871, People’s Republic of China; Center of Single-Molecule Sciences, Institute of Modern Optics, Frontiers Science Center for New Organic Matter, College of Electronic Information and Optical Engineering, Nankai University, Tianjin 300350, People’s Republic of China; [orcid.org/0000-0001-5723-8528](https://orcid.org/0000-0001-5723-8528); Email: [guoxf@pku.edu.cn](mailto:guoxf@pku.edu.cn)

### Authors

**Yilin Guo** – Beijing National Laboratory for Molecular Sciences, National Biomedical Imaging Center, College of Chemistry and Molecular Engineering, Peking University, Beijing 100871, People’s Republic of China

**Chen Yang** – Beijing National Laboratory for Molecular Sciences, National Biomedical Imaging Center, College of Chemistry and Molecular Engineering, Peking University, Beijing 100871, People’s Republic of China

**Huiping Li** – ICQD, Hefei National Laboratory for Physical Sciences at the Microscale, Department of Physics, University of Science and Technology of China, Anhui 230026, People’s Republic of China

**Lei Zhang** – School of Materials Science and Engineering, Peking University, Beijing 100871, People’s Republic of China; [orcid.org/0000-0001-9031-4318](https://orcid.org/0000-0001-9031-4318)

**Shuyao Zhou** – Beijing National Laboratory for Molecular Sciences, National Biomedical Imaging Center, College of Chemistry and Molecular Engineering, Peking University, Beijing 100871, People’s Republic of China

**Xin Zhu** – Center of Single-Molecule Sciences, Institute of Modern Optics, Frontiers Science Center for New Organic Matter, College of Electronic Information and Optical Engineering, Nankai University, Tianjin 300350, People’s Republic of China

**Huanyan Fu** – Center of Single-Molecule Sciences, Institute of Modern Optics, Frontiers Science Center for New Organic Matter, College of Electronic Information and Optical Engineering, Nankai University, Tianjin 300350, People’s Republic of China

**Zhizhou Li** – Beijing National Laboratory for Molecular Sciences, National Biomedical Imaging Center, College of Chemistry and Molecular Engineering, Peking University, Beijing 100871, People’s Republic of China

**Zhirong Liu** – Beijing National Laboratory for Molecular Sciences, National Biomedical Imaging Center, College of Chemistry and Molecular Engineering, Peking University, Beijing 100871, People’s Republic of China; [orcid.org/0000-0001-5070-8048](https://orcid.org/0000-0001-5070-8048)

**Chuancheng Jia** – Center of Single-Molecule Sciences, Institute of Modern Optics, Frontiers Science Center for New Organic Matter, College of Electronic Information and Optical Engineering, Nankai University, Tianjin 300350, People’s Republic of China

Complete contact information is available at: <https://pubs.acs.org/doi/10.1021/jacs.1c12490>

### Author Contributions

<sup>▽</sup>Y.G., C.Y., H.L., and L.Z. contributed equally to this work.

### Notes

The authors declare no competing financial interest.

## ■ ACKNOWLEDGMENTS

We thank Professor Michael C. Young from the University of Toledo very much for his helpful discussion and English editing. We acknowledge primary financial support from the National Key R&D Program of China (2017YFA0204901 and 2021YFA1200101), the National Natural Science Foundation of China (21727806, 21933001, 22150013, 22173050, and 21933012), the Tencent Foundation through the XPLOER PRIZE, Beijing National Laboratory for Molecular Sciences (BNLM202010) and Frontiers Science Center for New Organic Matter at Nankai University (63181206). S.Z. and Z.L. appreciate the support from the High-Performance Computing Platform of the Center for Life Science at Peking University.

## REFERENCES

- (1) Anslyn, E.; Dougherty, D. Experiments related to thermodynamics and kinetics. In *Modern Physical Organic Chemistry*; University Science Books: 2004; pp 421–488.
- (2) Westheimer, F. H. The magnitude of the primary kinetic isotope effect for compounds of hydrogen and deuterium. *Chem. Rev.* **1961**, *61*, 265–273.
- (3) Lee, I. Secondary kinetic isotope effects involving deuterated nucleophiles. *Chem. Soc. Rev.* **1995**, *24*, 223–229.
- (4) Kwan, E. E.; Zeng, Y. W.; Besser, H. A.; Jacobsen, E. N. Concerted nucleophilic aromatic substitutions. *Nat. Chem.* **2018**, *10*, 917–923.
- (5) Plata, R. E.; Singleton, D. A. A case study of the mechanism of alcohol-mediated Morita Baylis-Hillman reactions. The importance of experimental observations. *J. Am. Chem. Soc.* **2015**, *137*, 3811–3826.
- (6) Schuler, F. W.; Murphy, G. W. The kinetics of the rearrangement of vinyl allyl ether. *J. Am. Chem. Soc.* **1950**, *72*, 3155–3159.
- (7) Gajewski, J. J.; Conrad, N. D. Aliphatic Claisen rearrangement transition-state structure from secondary alpha-deuterium isotope effects. *J. Am. Chem. Soc.* **1979**, *101*, 2747–2748.
- (8) Meyer, M. P.; DelMonte, A. J.; Singleton, D. A. Reinvestigation of the isotope effects for the Claisen and aromatic Claisen rearrangements: The nature of the Claisen transition states. *J. Am. Chem. Soc.* **1999**, *121*, 10865–10874.
- (9) Gajewski, J. J. The Claisen rearrangement. Response to solvents and substituents: The case for both hydrophobic and hydrogen bond acceleration in water and for a variable transition state. *Acc. Chem. Res.* **1997**, *30*, 219–225.
- (10) Gajewski, J. J.; Brichford, N. L. Secondary deuterium kinetic isotope effects in the aqueous Claisen rearrangement: Evidence against an ionic transition state. *J. Am. Chem. Soc.* **1994**, *116*, 3165–3166.
- (11) Wiest, O.; Black, K. A.; Houk, K. N. Density functional theory isotope effects and activation energies for the Cope and Claisen rearrangements. *J. Am. Chem. Soc.* **1994**, *116*, 10336–10337.
- (12) Kupczyk-Subotkowska, L.; Saunders, W. H.; Shine, H. J.; Subotkowski, W. Thermal rearrangement of allyl vinyl ether: Heavy-atom kinetic isotope effects and the transition structure. *J. Am. Chem. Soc.* **1993**, *115*, 5957–5961.
- (13) McMichael, K. D.; Korver, G. L. Secondary deuterium isotope effects and transition state structure in the aromatic Claisen rearrangement. *J. Am. Chem. Soc.* **1979**, *101*, 2746–2747.
- (14) Wiest, O.; Houk, K. N.; Black, K. A.; Thomas, B. Secondary kinetic isotope effects of diastereotopic protons in pericyclic reactions: A new mechanistic probe. *J. Am. Chem. Soc.* **1995**, *117*, 8594–8599.
- (15) Yoo, H. Y.; Houk, K. N. Transition structures and kinetic isotope effects for the Claisen rearrangement. *J. Am. Chem. Soc.* **1994**, *116*, 12047–12048.
- (16) Gonzalez-Lafont, A.; Lluch, J. M. Kinetic isotope effects in chemical and biochemical reactions: Physical basis and theoretical methods of calculation. *WIREs Comput. Mol. Sci.* **2016**, *6*, 584–603.
- (17) Barkai, E.; Jung, Y. J.; Silbey, R. Theory of single-molecule spectroscopy: Beyond the ensemble average. *Annu. Rev. Phys. Chem.* **2004**, *55*, 457–507.
- (18) Lu, H. P.; Xun, L. Y.; Xie, X. S. Single-molecule enzymatic dynamics. *Science* **1998**, *282*, 1877–1882.
- (19) Zrimsek, A. B.; Chiang, N. H.; Mattei, M.; Zaleski, S.; McAnally, M. O.; Chapman, C. T.; Henry, A. I.; Schatz, G. C.; Van Duyne, R. P. Single-molecule chemistry with surface- and tip-enhanced Raman spectroscopy. *Chem. Rev.* **2017**, *117*, 7583–7613.
- (20) Florin, E. L.; Moy, V. T.; Gaub, H. E. Adhesion forces between individual ligand-receptor pairs. *Science* **1994**, *264*, 415–417.
- (21) Liu, C. M.; Kubo, K. R.; Wang, E. D.; Han, K. S.; Yang, F.; Chen, G. Q.; Escobedo, F. A.; Coates, G. W.; Chen, P. Single polymer growth dynamics. *Science* **2017**, *358*, 352–355.
- (22) Xiang, D.; Wang, X. L.; Jia, C. C.; Lee, T.; Guo, X. F. Molecular-scale electronics: From concept to function. *Chem. Rev.* **2016**, *116*, 4318–4440.
- (23) Chen, H. L.; Stoddart, J. F. From molecular to supramolecular electronics. *Nat. Rev. Mater.* **2021**, *6*, 804–828.
- (24) Song, H.; Kim, Y.; Jang, Y. H.; Jeong, H.; Reed, M. A.; Lee, T. Observation of molecular orbital gating. *Nature* **2009**, *462*, 1039–1043.
- (25) Liang, W. J.; Shores, M. P.; Bockrath, M.; Long, J. R.; Park, H. Kondo resonance in a single-molecule transistor. *Nature* **2002**, *417*, 725–729.
- (26) Park, J.; Pasupathy, A. N.; Goldsmith, J. I.; Chang, C.; Yaish, Y.; Petta, J. R.; Rinkoski, M.; Sethna, J. P.; Abruna, H. D.; McEuen, P. L.; Ralph, D. C. Coulomb blockade and the Kondo effect in single-atom transistors. *Nature* **2002**, *417*, 722–725.
- (27) Perrin, M. L.; Frisenda, R.; Koole, M.; Seldenthuis, J. S.; Gil, J. A. C.; Valkenier, H.; Hummelen, J. C.; Renaud, N.; Grozema, F. C.; Thijssen, J. M.; Dulic, D.; van der Zant, H. S. J. Large negative differential conductance in single-molecule break junctions. *Nat. Nanotechnol.* **2014**, *9*, 830–834.
- (28) Guedon, C. M.; Valkenier, H.; Markussen, T.; Thygesen, K. S.; Hummelen, J. C.; van der Molen, S. J. Observation of quantum interference in molecular charge transport. *Nat. Nanotechnol.* **2012**, *7*, 305–308.
- (29) Nguyen, Q. V.; Frisbie, C. D. Hopping conductance in molecular wires exhibits a large heavy-atom kinetic isotope effect. *J. Am. Chem. Soc.* **2021**, *143*, 2638–2643.
- (30) Li, Y.; Yang, C.; Guo, X. F. Single-molecule electrical detection: A promising route toward the fundamental limits of chemistry and life science. *Acc. Chem. Res.* **2020**, *53*, 159–169.
- (31) Xin, N.; Guan, J. X.; Zhou, C. G.; Chen, X. J. N.; Gu, C. H.; Li, Y.; Ratner, M. A.; Nitzan, A.; Stoddart, J. F.; Guo, X. F. Concepts in the design and engineering of single-molecule electronic devices. *Nat. Rev. Phys.* **2019**, *1*, 211–230.
- (32) Jia, C. C.; Ma, B. J.; Xin, N.; Guo, X. F. Carbon electrode-molecule junctions: A reliable platform for molecular electronics. *Acc. Chem. Res.* **2015**, *48*, 2565–2575.
- (33) Jia, C. C.; Migliore, A.; Xin, N.; Huang, S. Y.; Wang, J. Y.; Yang, Q.; Wang, S. P.; Chen, H. L.; Wang, D. M.; Feng, B. Y.; Liu, Z. R.; Zhang, G. Y.; Qu, D. H.; Tian, H.; Ratner, M. A.; Xu, H. Q.; Nitzan, A.; Guo, X. F. Covalently bonded single-molecule junctions with stable and reversible photoswitched conductivity. *Science* **2016**, *352*, 1443–1445.
- (34) Yang, C.; Liu, Z. T.; Li, Y. W.; Zhou, S. Y.; Lu, C. X.; Guo, X. F.; Ramirez, M.; Zhang, Q. Z.; Li, Y.; Liu, Z. R.; Houk, K. N.; Zhang, D. Q.; Guo, X. F. Electric field-catalyzed single-molecule Diels-Alder reaction dynamics. *Sci. Adv.* **2021**, *7*, No. eabf0689.
- (35) Yang, C.; Zhang, L.; Li, H.; Guo, Y.; Jia, C.; Zhu, W.; Mo, F.; Guo, X. Single-molecule electrical spectroscopy of organocatalysis. *Matter* **2021**, *4*, 2874–2885.
- (36) Zhou, C.; Li, X. X.; Gong, Z. L.; Jia, C. C.; Lin, Y. W.; Gu, C. H.; He, G.; Zhong, Y. W.; Yang, J. L.; Guo, X. F. Direct observation of single-molecule hydrogen-bond dynamics with single-bond resolution. *Nat. Commun.* **2018**, *9*, 807.
- (37) Wen, H. M.; Li, W. G.; Chen, J. W.; He, G.; Li, L. H.; Olson, M. A.; Sue, A. C. H.; Stoddart, J. F.; Guo, X. F. Complex formation dynamics in a single-molecule electronic device. *Sci. Adv.* **2016**, *2*, No. e1601113.
- (38) Liu, Z. H.; Li, X. X.; Masai, H.; Huang, X. Y.; Tsuda, S.; Terao, J.; Yang, J. L.; Guo, X. F. A single-molecule electrical approach for amino acid detection and chirality recognition. *Sci. Adv.* **2021**, *7*, No. eabe4365.
- (39) Rust, M. J.; Bates, M.; Zhuang, X. W. Sub-diffraction-limit imaging by stochastic optical reconstruction microscopy (STORM). *Nat. Methods* **2006**, *3*, 793–795.
- (40) Pincock, A. L.; Pincock, J. A.; Stefanova, R. Substituent effects on the rate constants for the photo-Claisen rearrangement of allyl aryl ethers. *J. Am. Chem. Soc.* **2002**, *124*, 9768–9778.
- (41) Gajewski, J. J.; Gee, K. R.; Jurayj, J. Energetic and rate effects of the trifluoromethyl group at C-2 and C-4 on the aliphatic Claisen rearrangement. *J. Org. Chem.* **1990**, *55*, 1813–1822.

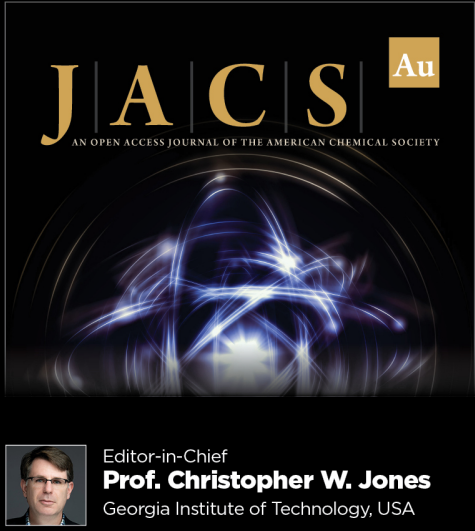
(42) Kwart, H. Temperature dependence of the primary kinetic hydrogen isotope effect as a mechanistic criterion. *Acc. Chem. Res.* **1982**, *15*, 401–408.

(43) Gajewski, J. J.; Olson, L. P.; Tupper, K. J. Hydrogen-deuterium fractionation factors for hydrogen- $sp^2$  carbon bonds in olefins and allyl radicals. *J. Am. Chem. Soc.* **1993**, *115*, 4548–4553.

(44) Narayan, S.; Muldoon, J.; Finn, M. G.; Fokin, V. V.; Kolb, H. C.; Sharpless, K. B. “On water”: Unique reactivity of organic compounds in aqueous suspension. *Angew. Chem., Int. Ed.* **2005**, *44*, 3275–3279.

(45) Shaik, S.; Ramanan, R.; Danovich, D.; Mandal, D. Structure and reactivity/selectivity control by oriented-external electric fields. *Chem. Soc. Rev.* **2018**, *47*, 5125–5145.

(46) Aragonés, A. C.; Haworth, N. L.; Darwish, N.; Ciampi, S.; Bloomfield, N. J.; Wallace, G. G.; Diez-Perez, I.; Coote, M. L. Electrostatic catalysis of a Diels-Alder reaction. *Nature* **2016**, *531*, 88–91.



**JACS Au**  
AN OPEN ACCESS JOURNAL OF THE AMERICAN CHEMICAL SOCIETY

Editor-in-Chief  
**Prof. Christopher W. Jones**  
Georgia Institute of Technology, USA

**Open for Submissions** 

pubs.acs.org/jacsau  ACS Publications  
Most Trusted. Most Cited. Most Read.